ACS APPLIED MATERIALS & INTERFACES

www.acsami.org

Research Article

Electromagnetic Interference Shielding with 2D Copper Sulfide

Taehun Kim,[⊥] Sangyeon Pak,[⊥] Jungmoon Lim, Jae Seok Hwang, Kyung-Ho Park, Byung-Sung Kim,* and SeungNam Cha*

Cite This: *ACS Appl. Mater. Interfaces* 2022, 14, 13499–13506

Read Online

ACCESS | Metrics & More | Article Recommendations | Supporting Information

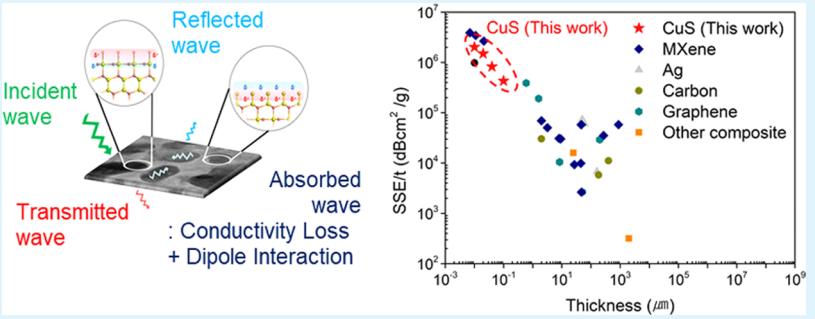

ABSTRACT: Electronic devices in highly integrated and miniaturized systems demand electromagnetic interference shielding within nanoscale dimensions. Although several ultrathin materials have been proposed, satisfying various requirements such as ultrathin thickness, optical transparency, flexibility, and proper shielding efficiency remains a challenge. Herein, we report an ultrahigh electromagnetic interference (EMI) SSE/*t* value (>10^6 dB cm^2/g) using a conductive CuS nanosheet with thickness less than 20 nm, which was synthesized at room temperature. We found that the EMI shielding efficiency (EMI SE) of the CuS nanosheet exceeds that of the traditional Cu film in the nanoscale thickness, which is due to high conductivity and the presence of internal dipole structures of the CuS nanosheet that contribute to absorption due to the damping of dipole oscillation. In addition, the CuS nanosheet exhibited high mechanical stability (10^4 cycles at 3 mm bending radius) and air stability (25 °C, 1 atm), which far exceeded the performance of the Cu nanosheet film. This remarkable performance of nanometer-thick CuS proposes an important pathway toward designing EMI shielding materials for wearable, flexible, and next-generation electronic applications.

KEYWORDS: *copper sulfide, CuS nanosheet, electromagnetic interference shielding, ultrathin thickness, dipole structures*

INTRODUCTION

The shrinking of the dimensions of electronic devices/components in the highly integrated system allowed electronic devices to be miniaturized, and the densities are ever-increasing. These devices and their components operate at faster speeds with closely spaced electronic components with different functions. Furthermore, the rapidly increasing demand for wearable electronics has resulted in electronic devices that come in close contact with the human body. Such devices that consume/distribute electrical energy create electromagnetic interference (EMI) and cause temporary disturbances or permanent failure to the highly sensitive, surrounding electronic systems by creating noise to the device input signals, thereby deteriorating the durability and proper functioning of the electronic equipment.[1−3] This electromagnetic pollution needs to be properly shielded not only to prevent malfunction in electronic components but also to block unwanted EM radiation to the surrounding environment and humans.[4]

EMI shielding materials must not only possess proper EMI shielding efficiency (SE) but also meet various requirements such as low-cost, lightweight, flexibility, and ultrathin thickness to broaden their applications, especially in the field that requires high packing density and/or flexible/wearable platforms. While high EMI SE can be conventionally achieved by employing conductive metals (e.g., Cu and Ag), maintaining such high SE values is difficult when the materials are designed to meet these requirements.[5] For example, Cu is a low-cost and highly conductive metal; however, for lightweight and flexible applications, employing an ultrathin Cu film has a limitation because it is susceptible to oxidation in air. Recently, metals[6−8] and other conducting nanomaterials[9,10] such as graphene[11−13] and MXene[14−24] were embedded into a polymer matrix for various lightweight and flexible EMI shielding applications. They showed high specific EMI shielding effectiveness (SSE)

Received: January 4, 2022
Accepted: March 1, 2022
Published: March 11, 2022

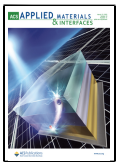

https://doi.org/10.1021/acsami.2c00196
ACS Appl. Mater. Interfaces 2022, 14, 13499−13506

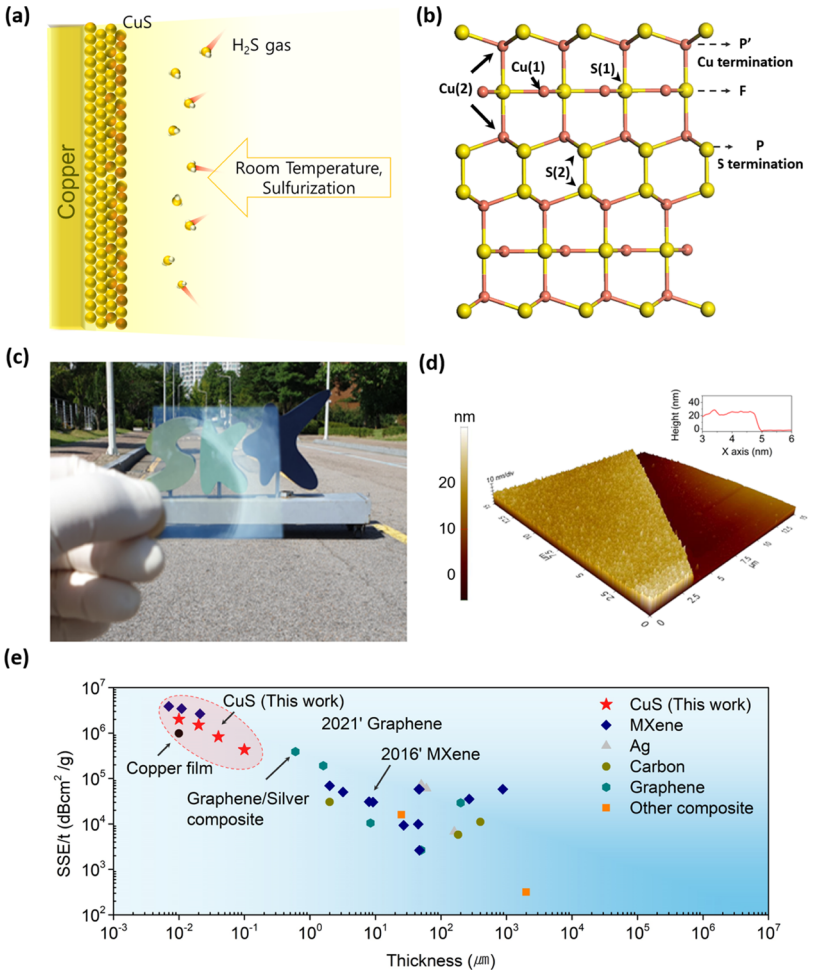

Figure 1. (a) Schematic illustration of a synthetic method of CuS nanosheet synthesis. The copper film was exposed to H_2S gas under ambient conditions. (b) Unit cell of hexagonal CuS. The red and yellow spheres are copper and sulfur atoms, respectively. (c) Optical image of the CuS nanosheet film (20 nm) deposited on a PET film. (d) 3D AFM topography image of the CuS nanosheet deposited on a SiO_2 substrate. The inset shows a cross-sectional 2D line profile of the CuS nanosheet. (e) EMI SSE/t versus thickness for the CuS nanosheet and other EMI shielding materials. Each symbol indicates a set of material categories as follows: Ag (gray triangle),[6−8] carbon (dark-yellow circle),[52−54] graphene (dark-cyan hexagon),[11−13] MXene (navy diamond),[14−24] and other composites, such as NiFe, Mo_2C (orange square).[9,10]

and SSE/t (SSE divided by thickness) values, which takes into consideration the material's density and thickness, respectively. While they are promising in terms of achieving flexibility, lightweight, and high EMI SE, the conductive nanomaterials have to be embedded into a polymer matrix, which hampers minimization of their thickness to meet various ultrathin applications. It is therefore difficult to find ultrathin materials that possess high shielding properties, flexibility, and transparency to meet various demands in electronic and wearable devices.

Herein, we show an ultrahigh EMI SSE/t value (>10^6 dB cm^2/g) using a flexible, transparent, air-stable, and ultrathin copper sulfide (CuS) nanosheet. To guarantee both mass and large-area production, the CuS nanosheet was prepared by a facile synthetic process at room temperature and ambient conditions, which enable the use of various substrates and form factors. Compared to previously fabricated CuS EMI shields,[25−37] the synthesized CuS nanosheet in this work is ultrathin, transparent, and large-sized continuous film consisting of CuS nanograin structures, which contributed to polarization loss associated with internal dipole structures, leading to increased absorption of EM waves. We found that the EMI SE of the CuS nanosheet exceeds that of conventional Cu film, which is attributed to the presence of myriad surface dipoles of the CuS nanocrystals as well as the high conductivity. The EMI shield made of the flexible and transparent CuS film shows high stability (>95%) in the EMI SE under repeated bending tests up to 10^4, outstanding transmittance above 80% in the visible range, and air stability (>70%) over a period of 8 weeks. These findings demonstrate that the ultrathin CuS can be employed for various practical EMI shielding applications.

EXPERIMENTAL SECTION

The schematic illustration of the room temperature synthesis of CuS is shown in Figure 1a. The CuS nanosheet was synthesized by sulfurizing a Cu film (<20 nm) using an ammonium sulfide ($(NH_4)_2S$) solution that generates H_2S gas in ambient conditions. At first, Cu reacts strongly with H_2S gas by forming the Cu_2S phase ($H_2S + 2Cu + 1/2O_2 \rightarrow Cu_2S + H_2O$). A continuous supply of H_2S gas then leads sulfur to diffuse further through sulfur vacancies and results in the formation of the covellite CuS phase.[38,39] The covellite CuS structure belongs to the space group $P63/mmc$, which is a hexagonal symmetry with 12 atoms in the unit cell (Figure 1b). It has a sandwich structure that is built up of a layer consisting of CuS_3 triangles and CuS_4 tetrahedra (CuS_4−CuS_3−CuS_4), the layer being connected with its adjacent structure by the S−S bond to attain the

https://doi.org/10.1021/acsami.2c00196
ACS Appl. Mater. Interfaces 2022, 14, 13499−13506

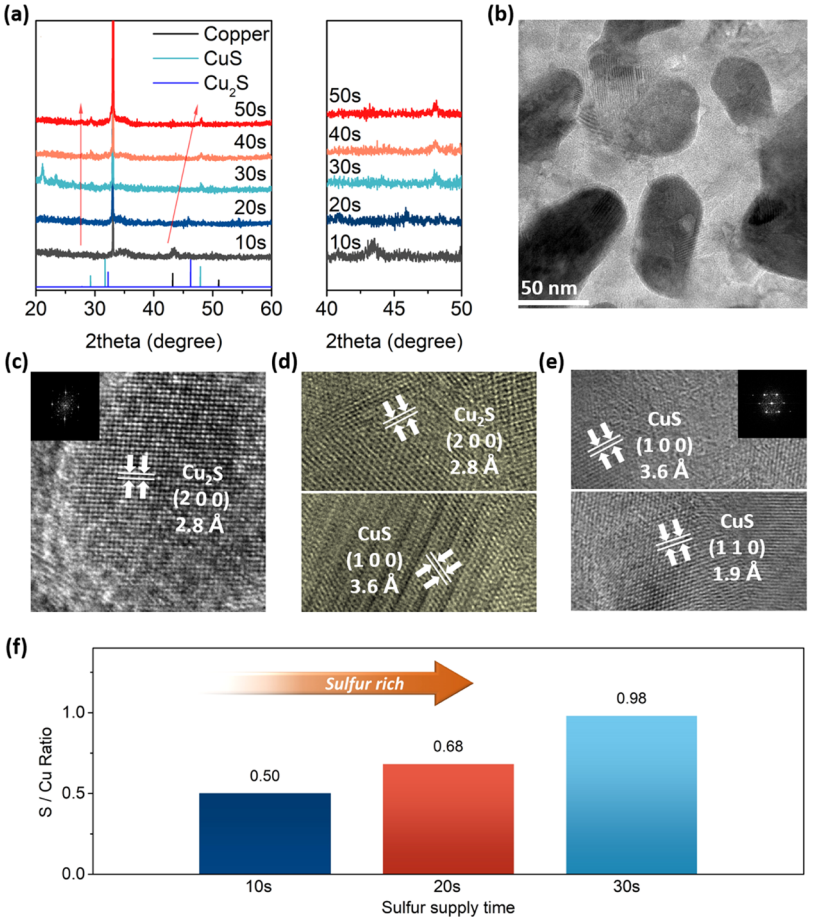

Figure 2. (a) XRD patterns of the CuS nanosheet with varying sulfurization times. For comparison, the standard XRD patterns of covellite (CuS, JCPDS No. 06-0464) and chalcocite (Cu_2S, JCPDS. No. 02-1294) are exhibited. Peaks at 33° correspond to the Si (200) plane. (b) TEM images of the copper sulfide with different sulfur supply times of (c) 10 s, (d) 20 s, and (e) 30 s. The insets show each selected-area electron diffraction (SAED) pattern. Sufficient sulfurization time leads to the CuS phase. (f) Cu/S ratio versus sulfur supply times. As the sulfurization time is increased, the ratio of the two atoms becomes 1:1.

continuity of the structure. The sandwiched structure can be easily cleaved to atomically smooth terraces along the (001) basal planes.[40] It is known that the cleavage with the lowest surface energy is likely to occur at the cleavage plane 1 (Cu(2) terminations) and plane 2 (S(1) terminations) shown in Figure 1b, which create dipolar layers perpendicular to the plane[41,42] that can contribute to enhanced EMI shielding performance.

Copper sulfide has been frequently employed as the conductive filler in the form of bulk powders or particles in EMI shielding polymer composites (thickness in the range of 80 nm to 3.5 mm).[25,28,29,31,32,35] Such bulk copper sulfide structures can vary widely in composition and crystal structures and do not show impressive EMI SE (32−45 dB in mm scale), which limits their wide range of applications.[25,28] It should be noted that in this work, we employed a covellite CuS film that shows impressive EMI shielding performance, while its thickness is much thinner than the CuS/polymer composite as compared in Table S1. The CuS nanosheet, which was prepared by a facile room temperature and ambient condition synthesis method, can guarantee a large-area production and enable the use of various substrates and form factors such as glass and flexible polymer substrates. Our ultrathin CuS film (20 nm) has high optical transmittance, as shown in the optical image in Figure 1c, and high electrical conductivity while maintaining the ultrathin thickness below 20 nm (the thickness was measured through AFM in Figure 1d), which is suitable as an EMI shield for transparent, flexible, and ultrathin applications.[43]

To evaluate the EMI performance of the ultrathin CuS nanosheet, we measured EMI transmittance and reflectance with a network vector analyzer (NVA, Keysight/Agilent E8364B) and compared it with other material's specific EMI shielding effectiveness (SSE, EMI SE/density (dB cm^3g^{-1})) versus thickness (SSE/t, Figure 1e) as this parameter allows fair comparison between different EMI shields that have different thicknesses. Surprisingly, the SSE/t values for the CuS nanosheet are much higher than those for other EMI shielding materials, including metals, 2D materials, and inorganic composites, and the SSE/t value of our CuS nanosheet reached up to 2.02×10^6 dB cm^2 g^{-1}. Recent studies report that MXene composites show a superior SSE/t value of 30 830 dB cm^2 g^{-1} with a micrometer thickness.[22] However, our CuS nanosheet has a much thinner thickness (20 nm) with ultrahigh SSE/t. Furthermore, the CuS nanosheet with 10 nm thickness has a higher SSE/t value than that of the Cu film with 10 nm thickness.

RESULTS AND DISCUSSION

To achieve high SSE/t values, it is highly important to precisely control and optimize the synthetic procedures and the corresponding crystal structure as copper sulfides exist in different phases and show different electrical properties. To investigate the origin of such high SSE/t values of the CuS nanosheet, we first analyzed the structure of the CuS nanosheet by X-ray diffraction (XRD) and high-resolution transmission electron microscopy (HRTEM). Figure 2a shows the XRD patterns of the 10 nm CuS nanosheet for various sulfurization times. From the XRD plots, it can be observed

https://doi.org/10.1021/acsami.2c00196
ACS Appl. Mater. Interfaces 2022, 14, 13499−13506

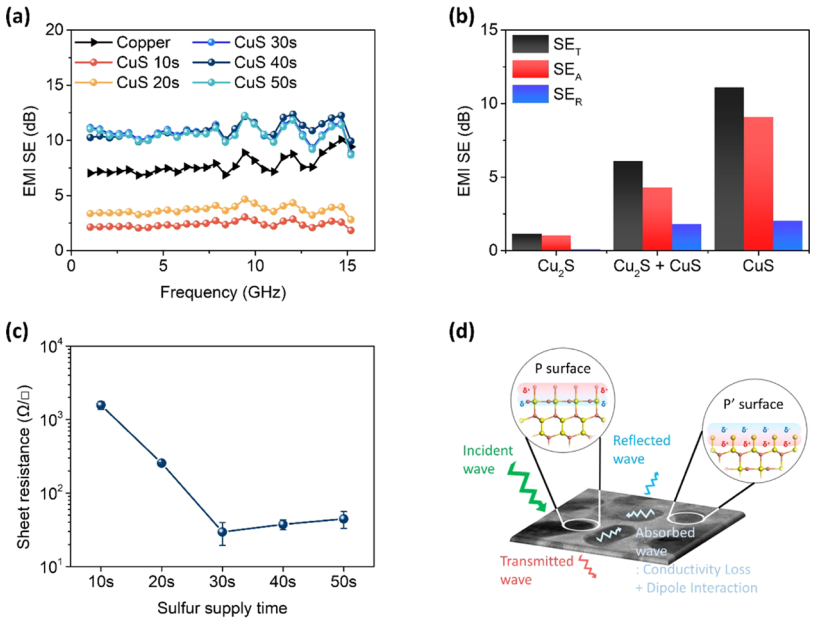

Figure 3. (a) EMI SE of the CuS under different sulfur supply times. (b) Total EMI SE (SE_T) and its absorption (SE_A) and reflection (SE_R) at 8.2 GHz. (c) Sheet resistance versus sulfur supply time. Low sheet resistance (29 Ω/□) was measured for the CuS nanosheet with a sulfurization time of 30 s or more. (d) Schematic illustration of the EM wave absorption mechanism. When an incident electric field interacts with dipoles present in the material, dipoles align themselves with respect to the electric field, leading to a damped oscillation.[57]

that for increased sulfurization time in the range of 10−50 s, phase changes from Cu to the Cu_2S and CuS were found. It should be noted that in the EMI shielding application, the CuS phase is more preferable to the Cu_2S phase due to the higher conductivity of CuS than that of Cu_2S.[44] When Cu was sulfurized for 10 s, the XRD peak corresponding to Cu was the dominant peak, while a new peak appeared at 46° when the sulfurization time was increased to 20 s, which corresponds to the Cu_2S (2 2 0) lattice (JCPDS No. 02-1294). As the sulfurization time was increased further to 30 s, the peak of the Cu_2S (2 2 0) lattice at 46° vanished, and new peaks at 29 and 48°, which correspond to the CuS (1 0 2) and (1 1 0) lattices (JCPDS No. 06-0464), respectively, were observed. Such trend of phase transition is in accordance with the shift of Raman spectrum measured for the CuS nanosheet with various sulfurization times, as shown in Figure S1.[45,46] The evolution of the crystal structure saturates at the sulfurization time of 30 s, and an additional sulfurization time with sufficient sulfur supply from H_2S gas guarantees the CuS phase to be dominant over the nanosheet film.

To further support the evolution of the crystal structure from Cu to CuS, the HRTEM measurements were performed for the CuS nanosheet with increasing sulfur supply time. Figure 2b shows the TEM image of the 10 nm CuS nanosheet, which is sulfurized for 30 s (30 s-CuS, hereafter), having a planar surface and small grains. The HRTEM analysis was further performed for the CuS nanosheet with different sulfurization times. Figure 2c−f shows the HRTEM images of the CuS nanosheets sulfurized for 10, 20, and 30 s, respectively, and the inset images are the SAED patterns extracted from each TEM image. The TEM image of the 10 s-CuS nanosheet shows that the Cu_2S phase is dominant over the entire nanosheet. It can be seen that the spacing is 0.28 nm, corresponding to the (2 0 0) d-spacing of the Cu_2S phase (Figure 2c). Figure 2d shows the TEM image of the 20 s-CuS nanosheet, where the phase Cu_2S to CuS coexist in the film. The TEM image of 30 s-CuS (Figure 2e) has the CuS phase, and then the *d*-spacing of 0.157 nm corresponds to the (1 0 2) lattice and that of 0.19 nm corresponds to the (1 1 0) lattice of covellite. Therefore, it shows that as the sulfurization time is increased, the Cu changes to Cu_2S, at first, and gradually changes to the CuS phase, implying that the optimization of sulfurization time is necessary for achieving the CuS crystal structure. To further understand the crystal phase and the elemental composition upon the sulfurization time, we measured energy-dispersive spectrometry (EDS), as shown in Figure 2f, which shows the copper-to-sulfur ratio under different sulfur supplies. As shown in the graph, the S/Cu ratio changes from 0.5 for the 10 s-CuS nanosheet to nearly 1 for the 30 s-CuS nanosheet, which corresponds to the CuS phase. The results measured through EDS analysis are in accordance with the phase transition observed through XRD, Raman, and HRTEM measurements.

Having confirmed the optimization of the CuS crystal structure upon sulfurization, we focus on the nature of EMI shielding performance in the CuS nanosheet. To explore the EMI shielding properties of the CuS nanosheet, we compared the EMI shielding effectiveness of the Cu film with that of the 20 nm CuS nanosheets, which are treated with various sulfurization times, as shown in Figure 3a. The 10 s-CuS nanosheet, which corresponds to the Cu_2S phase in XRD patterns, shows a SE_T of 2 dB at 8.2 GHz. The EMI SE of the CuS nanosheet gradually increased from 2 to 10 dB as the sulfurization time increased from 10 to 50 s. It is noteworthy to mention that the EMI SE of the CuS nanosheet with a sulfurization time of 30 s or above is higher than that of the Cu film. The pure Cu film has an intrinsic CuO layer upon the air exposure of the film (Figure S2). The intrinsic CuO layer formation is a disadvantage for the EMI SE of Cu films because the CuO has a much higher resistivity than the pure Cu film. As a result, the CuS nanosheet shows higher EMI SE than the Cu film at the same nanoscale thickness. Furthermore, it was

https://doi.org/10.1021/acsami.2c00196
ACS Appl. Mater. Interfaces 2022, 14, 13499−13506

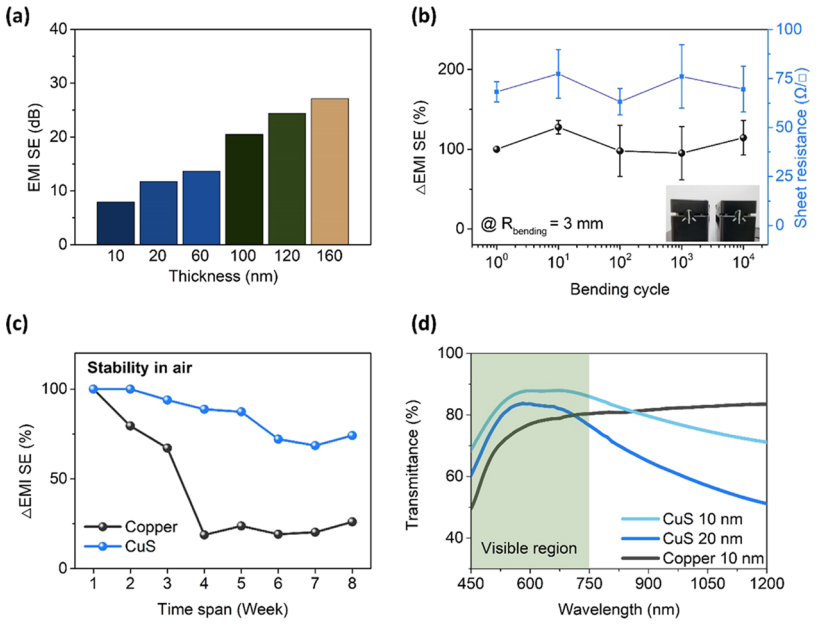

Figure 4. (a) EMI SE versus CuS thickness. (b) Mechanical stability test that monitors the EMI SE of bending radius and sheet resistance as bending cycles up to 10^4 at a 3 mm bending radius (secondary axis). (c) Cu and CuS nanosheet stability tests performed under room temperature conditions. (d) UV−vis transmittance spectra of the Cu film and the CuS nanosheet.

found that our CuS nanosheet shows similar EMI SE values at high and low frequencies and maintains excellent EMI shielding efficiency over the broad frequency range (500 MHz to 15 GHz).[47]

To gain fundamental insight into the nature of EMI shielding performance of the CuS nanosheet, we measured the S-parameter of the CuS nanosheet with different sulfurization times (we define as Cu_2S, Cu_2S/CuS, and CuS nanosheets for convenience), and the EMI SE_T, SE_R, and SE_A values at the 8.2 GHz were plotted, as shown in Figure 3b (also see the Supplementary Note 1). The total EMI SE (SE_T), consisting of reflection efficiency (SE_R), multiple reflection efficiency (SE_{MR}), and absorption efficiency (SE_A), can be described as follows

$$SE_{total}(dB) = SE_R + SE_A + SE_{MR} \approx SE_R + SE_A \quad (1)$$

$$SE_R(dB) = -10\log(1 - S_{11}^2) \quad (2)$$

$$SE_A(dB) = -10\log[S_{21}^2/(1 - S_{11}^2)] \quad (3)$$

In accordance with Figure 3a, the total EMI SE at a constant frequency of 8.2 GHz increases as the Cu to S ratio becomes 1:1, as shown in Figure 3b. It is also found that SE_A increases substantially from 0.8 to 7.6 dB, while the change of SE_R is relatively less significant as the crystal structure of the nanosheet evolves from Cu_2S to CuS. Furthermore, it can be seen that the contribution of absorption to the total EMI SE is significantly larger than that of reflection. In the CuS nanosheet, the SE_T, SE_A, and SE_R are found to be 9.8, 7.6, and 2.2 dB, respectively.

To further support the nature of the EMI shielding performance, a sheet resistance of the CuS nanosheet was measured with varying sulfurization times, as shown in Figure 3c. EMI shielding materials with low sheet resistance (i.e., high electrical conductivity, Figure S3) are typically needed to gain high EMI SE values. EMI SE can be expressed as follows

$$SE = 50 + 10\log\left(\frac{\sigma}{f}\right) + 1.7t\sqrt{\sigma f} \quad (4)$$

where σ is the electrical conductivity, f is the frequency, and t is the thickness of shielding material. In this regard, EMI SE shows a strong dependence on the electrical conductivity of the shielding material. A low sheet resistance in the CuS nanosheet was observed when the sulfurization time exceeded 30 s. The sheet resistance decreased from 1500 to 29 Ω/□, as the sulfurization time increased. Note that the resistance of the CuS nanosheet is similar to that of a commercial ITO film (10−30 Ω/□). Such low sheet resistance of the CuS nanosheet can be attributed to the stoichiometric balance of Cu and S atoms in $Cu_{2-x}S$, which affects the electrical properties of p-type conducting $Cu_{2-x}S$.[48,49] Therefore, the electrical properties can be enhanced by increasing the Cu/S ratio.

Such high EMI SE, even 20 nm thickness, can be attributed to enhanced dipole polarization loss due to the nanometer-sized grains and inherent dipole layers in the cleaved surfaces of CuS, as shown in Figure 3d. It has been theoretically predicted that surfaces with Cu and S terminations (depicted in Figure 1b) have the lowest surface energy, and due to the different terminations of the surface and different electronegativities of Cu and S atoms, the cleaved surfaces favor the formation of local surface dipole layers, which are depicted in Figure 3d.[41,42] Due to the small grain sizes of the CuS nanosheet, the polarization loss from surface dipole layers is greatly enhanced and contributes to increased absorption efficiency, which in turn improves the overall shielding performance (see Supplementary Note 2 for further explanations). Furthermore, CuS has a lower carrier concentration (~3 × 10^{21} cm^{-3}) than noble metals, which renders the Coulomb screening to be relatively reduced.[50] As a result, CuS has much faster electron−phonon scattering rates compared to conventional metals such as Au and Ag. The fast electron−phonon scattering associated with local carrier relaxation

https://doi.org/10.1021/acsami.2c00196
ACS Appl. Mater. Interfaces 2022, 14, 13499−13506

contributes to EM energy being more easily transformed into thermal energy or other forms of energy.[51]

The results presented clearly demonstrate the benefits of the crystal structure and morphology of the CuS nanosheet in realizing the ultrathin EMI shield. We now consider the feasibility of the CuS nanosheet in achieving practical, flexible, and transparent EMI shields. We, first, simply increased the thickness of the nanosheet to improve the EMI SE, as the thickness plays a crucial role in increasing the EMI SE of any material. We measured the EMI SE and sheet resistance of the CuS nanosheet with various film thicknesses, as shown in Figures 4a and S4, respectively. The EMI SE increased from 8.0 to 27.1 dB, as the film thickness increased from 10 to 160 nm. The highest EMI SE value of 27 was achieved when the film thickness increased to 160 nm, which is enough to block 99.8% of incident radiation with the CuS nanosheet. It should be noted that the CuS thickness shown in this work (10−160 nm) is much thinner than the thickness of previously reported composites (generally in the range of 1 μm to 2 mm).[6−11,14−24,52−54]

Because of the fast-growing wearable electronics field, the demand for an ultrathin and flexible EMI shielding film has recently increased dramatically. On the other hand, conductive metals are limited by their easy-corrosive and nonflexible characteristics, which are incompatible with the specifications of next-generation wearable electronics. Therefore, we investigated the mechanical stability and air stability of our flexible CuS nanosheet. For this, the changes in the EMI SE and sheet resistance were monitored in terms of the number of bending cycles and days. Figure 4b shows the mechanical stability test using our bending machine, and EMI SE and sheet resistance were measured after the multiple bending test. Upon 10^4 bending cycles, EMI SE was generated with only a slight variation in the magnitude (less than 5%). Furthermore, after multiple bending cycles, the sheet resistance was found to exhibit less than 10% degradation in the CuS nanosheet. In addition to the mechanical stability of the CuS nanosheet, the sheet resistance of the CuS film remained 74% of its original value over a period of 8 weeks when stored under ambient conditions with less than 50% humidity, as shown in Figure 4c. The surface of the CuS nanosheet can be slowly oxidized to $CuSO_4$ under ambient conditions (Figure S5).[55] By contrast, the EMI SE and sheet resistance of the 10 nm of Cu decreased and increased rapidly, respectively, as shown in Figures 4c and S6. After 4 weeks, the EMI SE value of Cu decreased by 25% of its original value due to the conversion of Cu into CuO (Figure S2).[56] These results suggest that the CuS has the strong merit for air stability compared to metals (e.g., copper) when their thicknesses are reduced to a nanometer range.

For their transparent EMI shielding applications, we measured the UV−vis transmittance spectra of CuS 20 nm nanosheets, which were measured in the visible to the infrared region (450−2500 nm), as shown in Figure 4d. It can be seen that the transmittance of the CuS nanosheet at 550 nm is above 80% and is clearly comparable to that of the 10 nm of copper. We also plotted transmittance versus SSE/t to compare the outstanding optical and EMI shielding properties with other EMI shielding materials, as shown in Figure S7. Based on this result, the CuS nanosheet is an appealing candidate for the EMI shield in transparent electronic devices.

CONCLUSIONS

To conclude, we have shown the outstanding EMI performance of ultrathin (<20 nm), highly conducting CuS nanosheets, which were synthesized simply by sulfurizing copper films at room temperature. We found that the reported EMI SSE/t values are the highest of any known shielding materials. We attribute such high performance to the evolution of the Cu film to a nano-sized covellite CuS structure with inherent dipole layers. Moreover, we showed that the CuS nanosheet has excellent mechanical properties, transparency, and air stability, which are important for their use in flexible and transparent electronic applications. Furthermore, this very thin shielding material is especially important for devices that need to be miniaturized. This study gives a new possibility for the CuS nanosheet in EMI shielding applications.

ASSOCIATED CONTENT

Supporting Information

The Supporting Information is available free of charge at https://pubs.acs.org/doi/10.1021/acsami.2c00196.

Material and method section; supplementary notes 1 and 2; Raman spectra, XRD patterns, and XPS spectra; sheet resistance of the CuS with various thicknesses; EMI SE value of the PI substrate; EMI SE and thickness of various EMI shielding materials; a plot of SSE/t versus transmittance; and absorption/reflection coefficient (PDF)

AUTHOR INFORMATION

Corresponding Authors

Byung-Sung Kim − *Materials & Devices Advanced Research Center, LG Electronics, Seoul 07796, Republic of Korea*; Email: bs2016.kim@lge.com

SeungNam Cha − *Department of Physics, Sungkyunkwan University (SKKU), Suwon, Gyeonggi-do 16419, Republic of Korea*; orcid.org/0000-0001-6284-8312; Email: chasn@skku.edu

Authors

Taehun Kim − *Department of Physics, Sungkyunkwan University (SKKU), Suwon, Gyeonggi-do 16419, Republic of Korea*

Sangyeon Pak − *School of Electronic and Electrical Engineering, Hongik University, Seoul 04066, Republic of Korea*; orcid.org/0000-0003-1765-3043

Jungmoon Lim − *Department of Physics, Sungkyunkwan University (SKKU), Suwon, Gyeonggi-do 16419, Republic of Korea*

Jae Seok Hwang − *Convergence Technology Division, Korea Advanced Nano Fab Center, Suwon, Gyeonggi-do 16229, Republic of Korea*

Kyung-Ho Park − *Convergence Technology Division, Korea Advanced Nano Fab Center, Suwon, Gyeonggi-do 16229, Republic of Korea*

Complete contact information is available at: https://pubs.acs.org/10.1021/acsami.2c00196

Author Contributions

$^{\perp}$T.K. and S.P. contributed equally to this work.

Notes

The authors declare no competing financial interest.

https://doi.org/10.1021/acsami.2c00196
ACS Appl. Mater. Interfaces 2022, 14, 13499−13506

■ ACKNOWLEDGMENTS

This work was supported by the National Research Foundation (NRF) of Korea (2019R1A2C1005930). S.P. thanks the financial support by Nano Material Technology Development Program through the NRF funded by the Ministry of Science, ICT and Future Planning (2009-0082580) and SKKU Supreme Research Program.

■ REFERENCES

(1) Yan, D. X.; Pang, H.; Li, B.; Vajtai, R.; Xu, L.; Ren, P. G.; Wang, J. H.; Li, Z. M. Structured Reduced Graphene Oxide/Polymer Composites for Ultra-Efficient Electromagnetic Interference Shielding. *Adv. Funct. Mater.* **2015**, *25*, 559−566.

(2) Chen, Z.; Xu, C.; Ma, C.; Ren, W.; Cheng, H. M. Lightweight and flexible graphene foam composites for high-performance electromagnetic interference shielding. *Adv. Mater.* **2013**, *25*, 1296−1300.

(3) Yousefi, N.; Sun, X.; Lin, X.; Shen, X.; Jia, J.; Zhang, B.; Tang, B.; Chan, M.; Kim, J. K. Highly aligned graphene/polymer nanocomposites with excellent dielectric properties for high-performance electromagnetic interference shielding. *Adv. Mater.* **2014**, *26*, 5480−5487.

(4) Frey, A. H. Headaches from cellular telephones: are they real and what are the implications? *Environ. Health Perspect.* **1998**, *106*, 101−103.

(5) Das, N. C.; Liu, Y.; Yang, K.; Peng, W.; Maiti, S.; Wang, H. Single-walled carbon nanotube/poly(methyl methacrylate) composites for electromagnetic interference shielding. *Polym. Eng. Sci.* **2009**, *49*, 1627−1634.

(6) Wang, Y. T.; Peng, H. K.; Li, T. T.; Shiu, B. C.; Zhang, X. F.; Lou, C. W.; Lin, J. H. Layer-by-layer assembly of low-temperature in-situ polymerized pyrrole coated nanofiber membrane for high-efficiency electromagnetic interference shielding. *Prog. Org. Coat.* **2020**, *147*, No. 105861.

(7) Wang, Y.; Peng, H.-K.; Li, T.-T.; Shiu, B.-C.; Zhang, X.; Lou, C.-W.; Lin, J.-H. Tuning lightweight, flexible, self-cleaning bio-inspired core−shell structure of nanofiber films for high-performance electromagnetic interference shielding. *J. Mater. Sci.* **2020**, *55*, 13008−13022.

(8) Li, T. T.; Wang, Y. T.; Peng, H. K.; Zhang, X. F.; Shiu, B. C.; Lin, J. H.; Lou, C. W. Lightweight, flexible and superhydrophobic composite nanofiber films inspired by nacre for highly electromagnetic interference shielding. *Composites, Part A* **2020**, *128*, No. 105685.

(9) Liu, X.; Xu, H.; Xie, F.; Fasel, C.; Yin, X.; Riedel, R. Highly flexible and ultrathin Mo2C film via in-situ growth on graphene oxide for electromagnetic shielding application. *Carbon* **2020**, *163*, 254−264.

(10) Yadav, R. S.; Kuritka, I.; Vilcakova, J.; Machovsky, M.; Skoda, D.; Urbanek, P.; Masar, M.; Jurca, M.; Urbanek, M.; Kalina, L.; Havlica, J. NiFe2O4 Nanoparticles Synthesized by Dextrin from Corn-Mediated Sol-Gel Combustion Method and Its Polypropylene Nanocomposites Engineered with Reduced Graphene Oxide for the Reduction of Electromagnetic Pollution. *ACS Omega* **2019**, *4*, 22069−22081.

(11) Wei, L.; Zhang, W.; Ma, J.; Bai, S.-L.; Ren, Y.; Liu, C.; Simion, D.; Qin, J. π-π stacking interface design for improving the strength and electromagnetic interference shielding of ultrathin and flexible water-borne polymer/sulfonated graphene composites. *Carbon* **2019**, *149*, 679−692.

(12) Lai, D.; Chen, X.; Wang, G.; Xu, X.; Wang, Y. Highly conductive porous graphene film with excellent folding resilience for exceptional electromagnetic interference shielding. *J. Mater. Chem. C* **2020**, *8*, 8904−8916.

(13) Liu, X.; Wu, W.; Guo, B.; Cui, M.; Ma, H.; Zhang, Z.; Zhang, R. Facile fabrication of ultrathin graphene film with ultrahigh electrical conductivity and superb electromagnetic interference shielding effectiveness. *J. Mater. Chem. C* **2021**, *9*, 214−222.

(14) Ma, C.; Cao, W.-T.; Zhang, W.; Ma, M.-G.; Sun, W.-M.; Zhang, J.; Chen, F. Wearable, ultrathin and transparent bacterial celluloses/MXene film with Janus structure and excellent mechanical property for electromagnetic interference shielding. *Chem. Eng. J.* **2021**, *403*, No. 126438.

(15) Bian, R.; He, G.; Zhi, W.; Xiang, S.; Wang, T.; Cai, D. Ultralight MXene-based aerogels with high electromagnetic interference shielding performance. *J. Mater. Chem. C* **2019**, *7*, 474−478.

(16) Miao, M.; Liu, R.; Thaiboonrod, S.; Shi, L.; Cao, S.; Zhang, J.; Fang, J.; Feng, X. Silver nanowires intercalating Ti3C2Tx MXene composite films with excellent flexibility for electromagnetic interference shielding. *J. Mater. Chem. C* **2020**, *8*, 3120−3126.

(17) Weng, C.; Xing, T.; Jin, H.; Wang, G.; Dai, Z.; Pei, Y.; Liu, L.; Zhang, Z. Mechanically robust ANF/MXene composite films with tunable electromagnetic interference shielding performance. *Composites, Part A* **2020**, *135*, No. 105927.

(18) Xin, W.; Xi, G.-Q.; Cao, W.-T.; Ma, C.; Liu, T.; Ma, M.-G.; Bian, J. Lightweight and flexible MXene/CNF/silver composite membranes with a brick-like structure and high-performance electromagnetic-interference shielding. *RSC Adv.* **2019**, *9*, 29636−29644.

(19) Weng, G.-M.; Li, J.; Alhabeb, M.; Karpovich, C.; Wang, H.; Lipton, J.; Maleski, K.; Kong, J.; Shaulsky, E.; Elimelech, M.; Gogotsi, Y.; Taylor, A. D. Layer-by-Layer Assembly of Cross-Functional Semi-transparent MXene-Carbon Nanotubes Composite Films for Next-Generation Electromagnetic Interference Shielding. *Adv. Funct. Mater.* **2018**, *28*, No. 1803360.

(20) Jin, X.; Wang, J.; Dai, L.; Liu, X.; Li, L.; Yang, Y.; Cao, Y.; Wang, W.; Wu, H.; Guo, S. Flame-retardant poly(vinyl alcohol)/MXene multilayered films with outstanding electromagnetic interference shielding and thermal conductive performances. *Chem. Eng. J.* **2020**, *380*, No. 122475.

(21) Raagulan, K.; Braveenth, R.; Jang, H. J.; Seon Lee, Y.; Yang, C. M.; Mi Kim, B.; Moon, J. J.; Chai, K. Y. Electromagnetic Shielding by MXene-Graphene-PVDF Composite with Hydrophobic, Lightweight and Flexible Graphene Coated Fabric. *Materials* **2018**, *11*, No. 1803.

(22) Shahzad, F.; Alhabeb, M.; Hatter, C. B.; Anasori, B.; Hong, S. M.; Koo, C. M.; Gogotsi, Y. Electromagnetic interference shielding with 2D transition metal carbides (MXenes). *Science* **2016**, *353*, 1137−1140.

(23) Cao, W. T.; Chen, F. F.; Zhu, Y. J.; Zhang, Y. G.; Jiang, Y. Y.; Ma, M. G.; Chen, F. Binary Strengthening and Toughening of MXene/Cellulose Nanofiber Composite Paper with Nacre-Inspired Structure and Superior Electromagnetic Interference Shielding Properties. *ACS Nano* **2018**, *12*, 4583−4593.

(24) Xiang, C.; Guo, R.; Lin, S.; Jiang, S.; Lan, J.; Wang, C.; Cui, C.; Xiao, H.; Zhang, Y. Lightweight and ultrathin TiO2-Ti3C2TX/graphene film with electromagnetic interference shielding. *Chem. Eng. J.* **2019**, *360*, 1158−1166.

(25) Zhang, X.-J.; Wang, G.-S.; Wei, Y.-Z.; Guo, L.; Cao, M.-S. Polymer-composite with high dielectric constant and enhanced absorption properties based on graphene−CuS nanocomposites and polyvinylidene fluoride. *J. Mater. Chem. A* **2013**, *1*, 12115−12122.

(26) Ghosh, K.; Srivastava, S. K. Enhanced Supercapacitor Performance and Electromagnetic Interference Shielding Effectiveness of CuS Quantum Dots Grown on Reduced Graphene Oxide Sheets. *ACS Omega* **2021**, *6*, 4582−4596.

(27) Chen, Y.-H.; Huang, C.-Y.; Lai, F.-D.; Roan, M.-L.; Chen, K.-N.; Yeh, J.-T. Electroless deposition of the copper sulfide coating on polyacrylonitrile with a chelating agent of triethanolamine and its EMI Shielding Effectiveness. *Thin Solid Films* **2009**, *517*, 4984−4988.

(28) Hu, X. S.; Shen, Y. Fabrication of novel polyaniline/flowerlike copper monosulfide composites with enhanced electromagnetic interference shielding effectiveness. *J. Appl. Polym. Sci.* **2017**, *134*, No. 45232.

(29) Biswas, S.; Dutta, S.; Panja, S. S.; Bose, S. Template-Free Synthesis of "Wool-Ball"-Like Hollow CuS Structures Can Effectively Suppress Electromagnetic Radiation: A Mechanistic Insight. *J. Phys. Chem. C* **2019**, *123*, 17136−17147.

https://doi.org/10.1021/acsami.2c00196
ACS Appl. Mater. Interfaces 2022, 14, 13499−13506

(30) Hu, X.-S.; Shen, Y.; Xu, L.-H.; Wang, L.-M.; Lu, L.-s.; Zhang, Y.-t. Preparation of flower-like CuS by solvothermal method for photocatalytic, UV protection and EMI shielding applications. *Appl. Surf. Sci.* **2016**, *385*, 162−170.
(31) Zhao, B.; Shao, G.; Fan, B.; Zhao, W.; Xie, Y.; Zhang, R. Synthesis of flower-like CuS hollow microspheres based on nanoflakes self-assembly and their microwave absorption properties. *J. Mater. Chem. A* **2015**, *3*, 10345−10352.
(32) He, S.; Wang, G.-S.; Lu, C.; Liu, J.; Wen, B.; Liu, H.; Guo, L.; Cao, M.-S. Enhanced wave absorption of nanocomposites based on the synthesized complex symmetrical CuS nanostructure and poly (vinylidene fluoride). *J. Mater. Chem. A* **2013**, *1*, 4685−4692.
(33) Sharma, D.; Menon, A. V.; Bose, S. Graphene templated growth of copper sulphide "flowers" can suppress electromagnetic interference. *Nanoscale Adv.* **2020**, *2*, 3292−3303.
(34) He, S.; Wang, G.-S.; Lu, C.; Luo, X.; Wen, B.; Guo, L.; Cao, M.-S. Controllable fabrication of CuS hierarchical nanostructures and their optical, photocatalytic, and wave absorption properties. *ChemPlusChem* **2013**, *78*, 250.
(35) Wei, Y.-Z.; Wang, G.-S.; Wu, Y.; Yue, Y.-H.; Wu, J.-T.; Lu, C.; Guo, L. Bioinspired design and assembly of platelet reinforced polymer films with enhanced absorption properties. *J. Mater. Chem. A* **2014**, *2*, 5516−5524.
(36) Liu, P.; Huang, Y.; Yan, J.; Yang, Y.; Zhao, Y. Construction of CuS nanoflakes vertically aligned on magnetically decorated graphene and their enhanced microwave absorption properties. *ACS Appl. Mater. Interfaces* **2016**, *8*, 5536−5546.
(37) Roan, M.-L.; Chen, Y.-H.; Liao, H.-H.; Huang, C.-Y.; Chen, K.-N.; Yeh, J.-T. Electroless Copper Sulfide Deposition on the Polyacrylonitrile Films with Chelating Agents and its EMI Shielding Effectiveness. *Macromol. Symp.* **2009**, *286*, 116−124.
(38) Sansregret, J. L. Reaction of Copper Oxide with H2S. *J. Electrochem. Soc.* **1980**, *127*, 2083.
(39) Reid, M.; Punch, J.; Ryan, C.; Garfias, L. F.; Belochapkine, S.; Franey, J. P.; Derkits, G. E.; Reents, W. D. Microstructural Development of Copper Sulfide on Copper Exposed to Humid H2S. *J. Electrochem. Soc.* **2007**, *154*, C209.
(40) Ren, Y.; Wei, H.; Yang, B.; Wang, J.; Ding, J. "Double-Sandwich-Like" CuS@reduced graphene oxide as an Anode in Lithium Ion Batteries with Enhanced Electrochemical Performance. *Electrochim. Acta* **2014**, *145*, 193−200.
(41) Tasker, P. The stability of ionic crystal surfaces. *J. Phys. C* **1979**, *12*, 4977.
(42) Soares, A. L.; Dos Santos, E. C.; Morales-García, Á.; Duarte, H. A.; DeAbreu, H. A. The Stability and Structural, Electronic and Topological Properties of Covellite (001) Surfaces. *ChemistrySelect* **2016**, *1*, 2730−2741.
(43) Li, S.; Zha, T.; Wang, Q.; Wang, C.; Ren, Y.; Chen, Y.; Pan, D. Facile fabrication of p-type Cu x S transparent conducting thin films by metal sulfide precursor solution approach and their application in quantum dot thin films. *J. Alloys Compd.* **2017**, *716*, 278−283.
(44) Jiang, K.; Chen, Z.; Meng, X. CuS and Cu2S as Cathode Materials for Lithium Batteries: A Review [A Review on CuS and Cu2S as Cathode Materials for Lithium Batteries]. *ChemElectroChem* **2019**, *6*, 2825−2840.
(45) Hong, J.; Kim, B. S.; Hou, B.; Pak, S.; Kim, T.; Jang, A. R.; Cho, Y.; Lee, S.; An, G. H.; Jang, J. E.; Morris, S. M.; Sohn, J. I.; Cha, S. Room Temperature Wafer-Scale Synthesis of Highly Transparent, Conductive CuS Nanosheet Films via a Simple Sulfur Adsorption-Corrosion Method. *ACS Appl. Mater. Interfaces* **2021**, *13*, 4244−4252.
(46) Pak, S.; Jang, S.; Kim, T.; Lim, J.; Hwang, J. S.; Cho, Y.; Chang, H.; Jang, A. R.; Park, K. H.; Hong, J.; Cha, S. Electrode-Induced Self-Healed Monolayer MoS2 for High Performance Transistors and Phototransistors. *Adv. Mater.* **2021**, *33*, No. 2102091.
(47) Wei, W.; Liu, X.; Lu, W.; Zhang, H.; He, J.; Wang, H.; Hou, Y. Light-weight Gadolinium Hydroxide@polypyrrole Rare-Earth Nanocomposites with Tunable and Broadband Electromagnetic Wave Absorption. *ACS Appl. Mater. Interfaces* **2019**, *11*, 12752−12760.
(48) Bekenstein, Y.; Vinokurov, K.; Keren-Zur, S.; Hadar, I.; Schilt, Y.; Raviv, U.; Millo, O.; Banin, U. Thermal doping by vacancy formation in copper sulfide nanocrystal arrays. *Nano Lett.* **2014**, *14*, 1349−1353.
(49) Grozdanov, I.; Najdoski, M. Optical and electrical properties of copper sulfide films of variable composition. *J. Solid State Chem.* **1995**, *114*, 469−475.
(50) Bykov, A. Y.; Shukla, A.; van Schilfgaarde, M.; Green, M. A.; Zayats, A. V. Ultrafast Carrier and Lattice Dynamics in Plasmonic Nanocrystalline Copper Sulfide Films. *Laser Photonics Rev.* **2021**, *15*, No. 2000346.
(51) Prasad, J.; Singh, A. K.; Haldar, K. K.; Gupta, V.; Singh, K. Electromagnetic interference shielding effectiveness in 3D flower-like MoS2-rGO/gadolinium-doped nanocomposites. *J. Alloys Compd.* **2019**, *788*, 861−872.
(52) Lu, D.; Mo, Z.; Liang, B.; Yang, L.; He, Z.; Zhu, H.; Tang, Z.; Gui, X. Flexible, lightweight carbon nanotube sponges and composites for high-performance electromagnetic interference shielding. *Carbon* **2018**, *133*, 457−463.
(53) Lee, J.; Liu, Y.; Liu, Y.; Park, S.-J.; Park, M.; Kim, H. Y. Ultrahigh electromagnetic interference shielding performance of lightweight, flexible, and highly conductive copper-clad carbon fiber nonwoven fabrics. *J. Mater. Chem. C* **2017**, *5*, 7853−7861.
(54) Xing, D.; Lu, L.; Xie, Y.; Tang, Y.; Teh, K. S. Highly flexible and ultra-thin carbon-fabric/Ag/waterborne polyurethane film for ultra-efficient EMI shielding. *Mater. Des.* **2020**, *185*, No. 108227.
(55) Wu, H.; Or, V. W.; Gonzalez-Calzada, S.; Grassian, V. H. CuS nanoparticles in humid environments: adsorbed water enhances the transformation of CuS to CuSO 4. *Nanoscale* **2020**, *12*, 19350−19358.
(56) Li, J.; Mayer, J.; Colgan, E. Oxidation and protection in copper and copper alloy thin films. *J. Appl. Phys.* **1991**, *70*, 2820−2827.
(57) Tretyakov, S. Maximizing Absorption and Scattering by Dipole Particles. *Plasmonics* **2014**, *9*, 935−944.

https://doi.org/10.1021/acsami.2c00196
ACS Appl. Mater. Interfaces 2022, 14, 13499−13506